Available online at www.sciencedirect.com
ScienceDirect
International Journal of Heat and Mass Transfer 51 (2008) 1439–1452
International Journal of HEAT and MASS TRANSFER
www.elsevier.com/locate/ijhmt

An efficient BEM formulation for three-dimensional steady-state heat conduction analysis of composites

J. Chatterjee, D.P. Henry, F. Ma, P.K. Banerjee *

Department of Civil Engineering, State University of New York at Buffalo, 240 Ketter Hall, Buffalo, NY 14260, USA

Received 6 September 2006; received in revised form 21 March 2007
Available online 26 October 2007

Abstract

In this work, an efficient boundary element formulation has been presented for three-dimensional steady-state heat conduction analysis of fiber reinforced composites. The cylindrical shaped fibers in the three-dimensional composite matrix are represented by a system of curvilinear line elements with a prescribed diameter which facilitates efficient analysis and modeling together with the reduction in dimensionality of the problem. The variations in the temperature and flux fields in the circumferential direction of the fiber are represented in terms of a trigonometric shape function together with a linear or quadratic variation in the longitudinal direction. The resulting integrals are then treated semi-analytically which reduces the computational task significantly. The computational effort is further minimized by analytically substituting the fiber equations into the boundary integral equation of the material matrix with hole, resulting in a modified boundary integral equation of the composite matrix. An efficient assembly process of the resulting system equations is demonstrated together with several numerical examples to validate the proposed formulation. An example of application is also included.

Keywords: Boundary element method; Composite; Heat conduction

1. Introduction

The heat flow in a composite is a complex phenomenon and can only be understood through a proper micromechanical analysis. A suitable numerical method can be used for this purpose in which the matrix and the fibers are modeled as separate regions. However, for a relatively large problem with numerous fibers, this type of approach is not very practical, because, very large amount of computing resources as well as significant amount of modeling efforts are necessary. Moreover, when fiber diameter becomes very small, multi-region approach often leads to inaccuracies particularly for a large difference in material properties, resulting in the coefficients in the system matrix differing by orders of magnitude. For this reason, one needs to use a numerical method in which the individual fibers or individual bundle of fibers can be idealized in an efficient manner within a three-dimensional (3D) matrix. At the same time, the analysis must be sophisticated enough to take into account of high temperature gradient resulting from the diffusion of temperature from the fiber to the matrix and allow for the interaction between the fibers.

Boundary element method (BEM) is almost uniquely favorable for this task. The reduction of dimensionality of the problem using BEM enables very efficient modeling and analysis when combined with an efficient idealization of the fibers within a matrix. Furthermore, developments of BEM over the years have shown generality and versatility of the method to successfully analyze 3D heat conduction problems [1–4].

There are many published papers written on heat transfer, elasticity and thermoelasticity that are described as papers on composites, but with a closer examination, one

* Corresponding author. Tel.: +1 716 645 2114x2426; fax: +1 716 645 3945.
E-mail address: pkb@eng.buffalo.edu (P.K. Banerjee).

0017-9310/$ - see front matter © 2007 Published by Elsevier Ltd.
doi:10.1016/j.ijheatmasstransfer.2007.09.004

Nomenclature

a_{ij}	direction cosines between the local and global coordinate system	N^{α}	longitudinal shape function
C	integration constant	Q	flux
F	temperature kernel	R	fiber radius
G	flux kernel	S	surface of the outer boundary
h	film coefficient	S^n	surface of the hole
k	conductivity	T	temperature
$L(\eta_i,\eta_i)$	boundary element shape function	T_{α}	the ambient temperature
M^{γ}	circular shape function	x_i	coordinates of integration point
n_i	normals in local coordinates	θ	angle
N	number of fibers	ξ_i	coordinates of field point
		η_i	local axes system

sees that these are really anisotropic BEM papers for homogeneous regions. Mostly these deal with two-dimensional (2D) applications but a few deal with 3D applications. While these are relevant for the global analyses of composites, one cannot regard these to be relevant for micromechanical studies of composites.

There are several 2D multi-region modeling papers involving regular BEM modeling of large inclusions within a matrix. Unfortunately, these analyses require that the inclusion remain large enough so that there is no evidence of any instability. Applications of these types can be found for heat transfer, elasticity as well as thermoelasticity. There are also a few papers that describe a few large inclusions within a three-dimensional body.

Some authors such as Nishimura and Liu [16] describe quite large single region BEM system with a large number of internal surfaces to which they apply insulated or rigid boundary conditions. These may look like composites, but in reality, these are holes in a 3D solid. In order to be relevant for composites, the analysis must include compressibility, flexibility and heat transfer through them by modeling the included regions with their material properties.

The only paper which deals with an elastic micromechanical analysis by BEM was published by Banerjee and Henry [6]. They recognized that in a multi-region BEM, one can only solve inclusion problems if the size of the elements on the surface of the region to that on the surface of the inclusion remains within a ratio of 100–1000 depending on the quality of the numerical implementation. For long thin fibers, one needs to focus on somehow treating the geometric features analytically. This observation led to the developed Fourier Series based shape functions used in the present work.

In this work, an efficient and simplified BEM formulation for steady-state heat conduction analysis of 3D solids with fiber inclusions has been developed. The cylindrical shaped fibers are idealized as a system of curvilinear line elements with a prescribed diameter. The variations in the temperature and flux fields are assumed in the circumferential direction in terms of a trigonometric shape function together with a linear or quadratic variation along the longitudinal direction. The resulting integrals are then semi-analytically integrated [5]. Based on the compatibility conditions on the interface of the fiber and the matrix, the equations for fibers are simplified and then analytically substituted into the boundary integral equation of the composite matrix with holes to produce a modified boundary integral for the problem. A very efficient assembly process of the system equations is then developed where the temperatures on the interfaces of the matrix and the fibers are eliminated through a back-substitution of the fiber equations into the system equations which are made up exclusively from equations written for the composite matrix (on the outer boundary surface and on the surface of the hole). The present analysis has been implemented in a general purpose multi-region BEM code and several numerical examples using the developed algorithm are presented.

2. Boundary integral equation formulation

Following usual procedures, the boundary integral equation for the temperature at a point ξ inside a 3D solid with a hole can be written as [1,3]

$$C(\xi)T(\xi) = \int_S [G^{\mathrm{O}}(x,\xi)q^{\mathrm{O}}(x) - F^{\mathrm{O}}(x,\xi)T^{\mathrm{O}}(x)]\,\mathrm{d}S(x) + \sum_{n=1}^{N}\int_{S^n}[G^{\mathrm{H}}(x,\xi)q^{\mathrm{H}}(x) - F^{\mathrm{H}}(x,\xi)T^{\mathrm{H}}(x)]\,\mathrm{d}S^n(x) \quad (1)$$

In the above expression, G, F are the fundamental solutions of the governing differential equations of the matrix of infinite extent [2] given by

$$G(x,\xi) = \frac{1}{4\pi r}\left(\frac{1}{k}\right) \quad \text{(Temperature kernel)}$$

$$F(x,\xi) = \frac{1}{4\pi r^2}\left[\frac{y_{\mathrm{k}}n_{\mathrm{k}}}{r}\right] \quad \text{(Flux kernel)}$$

where x_i is the coordinates of integration point and ξ_i is the coordinates of the field point, $y_i = x_i - \xi_i$, $r^2 = y_i y_i$.

$C(\xi)$ is a constant whose value is dependent on the geometry of the position of the point ξ; T and q are temperatures and fluxes, respectively; S, S^n are the surfaces of the outer boundary of the matrix and the nth hole (will be used later for fiber); N is the number of individual fibers. The superscripts O and H denote the quantities on the outer surface of the matrix and the quantities on the surface of the hole, respectively.

The conventional boundary integral equation for temperature can also be written for each of the N fibers. For, the temperature at a point ξ inside the nth fiber can be written as

$$C^{\mathrm{F}}(\xi)T(\xi) = \int_{S^n} [G^{\mathrm{F}}(x,\xi)q^{\mathrm{F}}(x) - F^{\mathrm{F}}(x,\xi)T^{\mathrm{F}}(x)]\,\mathrm{d}S^n(x) \quad (2)$$

In the above, G^{F}, F^{F} are the fundamental solutions of the nth fiber; $C^{\mathrm{F}}(\xi)$ is a constant whose value is dependent on the position of the point ξ in fiber n; T^{F}, q^{F} are temperatures and fluxes, respectively, associated with the nth fiber. S^n is the surfaces of the nth fiber. The superscripts F is used to denote the quantities on the surface of the fiber.

Next, we examine the interface conditions between the matrix and the fiber. For a perfect bond, in order to satisfy the compatibility conditions, the following relationships must hold

$$T^{\mathrm{H}}(x) = T^{\mathrm{F}}(x) \quad (3a)$$

$$q^{\mathrm{H}}(x) = -q^{\mathrm{F}}(x) \quad (3b)$$

Upon consideration of the surface normals at the interface and examination of F kernels, we can write the following relation for the nth fiber.

$$F^{\mathrm{F}}(x,\xi) = -F^{\mathrm{H}}(x,\xi) \quad (3c)$$

Substitution of Eqs. (3) into Eq. (2) yields the following modified boundary integral equation for fiber n.

$$C^{\mathrm{F}}(\xi)T(\xi) = \int_{S^n} [-G^{\mathrm{F}}(x,\xi)q^{\mathrm{H}}(x) + F^{\mathrm{H}}(x,\xi)T^{\mathrm{H}}(x)]\,\mathrm{d}S^n(x) \quad (4)$$

Finally adding N fiber Eqs. (4) into Eq. (1) and canceling terms, leads to the following modified boundary integral equation for the matrix with hole

$$\overline{C}(\xi)T(\xi) = \int_{S^n} [G^{\mathrm{O}}(x,\xi)q^{\mathrm{O}}(x) - F^{\mathrm{O}}(x,\xi)T^{\mathrm{O}}(x)]\,\mathrm{d}S^n(x) + \sum_{n=1}^{N} \int_{S^n} [\overline{G}(x,\xi)q^{\mathrm{H}}(x)]\,\mathrm{d}S^n(x) \quad (5)$$

where

$$\overline{G}(x,\xi) = G^{\mathrm{H}}(x,\xi) - G^{\mathrm{F}}(x,\xi) \quad (6)$$

In the above, $\overline{C}(\xi)$ is a constant dependent on the position of the point ξ.

3. Analytical integration around a fiber inclusion

In this work, we have adopted the semi-analytical integration procedure developed by Banerjee and Henry [5] for elastic analysis of 3D solids with small diameter fiber inclusions. Using this approach, the fibers modeled using fiber elements which are defined by describing the centerline of the tubular (or curvilinear) fiber with nodal points; defining the connectivity of the nodal points; and specifying the radius of the fiber at each of those nodal points (refer to Fig. 1). Internally the program generates the surface of the fiber and the hole in which the resulting temperatures and fluxes are represented using a trigonometric circular shape function in the circumferential direction and a curvilinear shape function of any order in the longitudinal direction. A curved fiber thus can be described by a number of fiber elements connected end to end, and any fiber element not connected to another is assumed to be closed at the end by a circular disc.

The essential part of the formulation is then to convert the 2D surface integration of the fiber (and of the hole) to a one-dimensional (1D) integration [6,7]. By performing an analytical integration of the fiber in the circumferential direction, the computational burden is significantly reduced and simple numerical integration of the resulting line element can be carried out in the longitudinal direction. We adopt this semi-analytical integration approach in our present implementation.

In order to perform an analytical integration in the circumferential direction, the 3D kernel functions are first expressed in local coordinates with the center of the coordinate system coinciding with the center of the fiber/hole and the z axis aligned with the centerline of the fiber. The relative translation ξ'_i is added to the field coordinate ξ_i and the rotation is applied using the following vector transformation.

$$\xi_i = a_{ij}\bar{\xi}_j + \xi'_i \quad (7)$$

where a_{ij} are the direction cosines between the axes of the local ($\bar{\xi}_j$) and global (ξ_i) coordinate systems and the bar denotes a local variable.

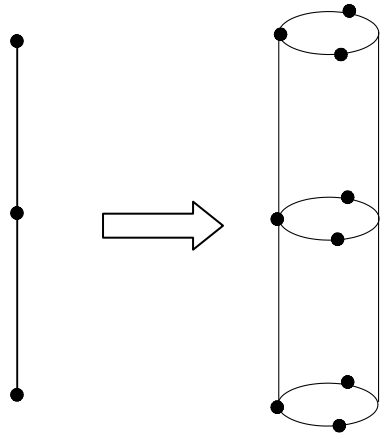

Fig. 1. Generation of the surface of the fiber (and the surface of the hole containing the fiber) from user input nodes.

The integration point x_i for a ring can thus be expressed in cylindrical coordinates relative to the center of the fiber/hole as

$$x_1 = R\cos\theta \quad x_2 = R\sin\theta \quad x_3 = 0 \tag{8}$$

where R represents the radius of the fiber with $R = (x_1^2 + x_2^2)^{1/2}$.

The normal vectors are transformed using

$$n_1 = n_r\cos\theta \quad n_2 = n_r\sin\theta \quad n_3 = n_z \tag{9}$$

where n_r and n_z represent the normals of the side of the hole in local coordinates and are dependent on the change in the radius of the fiber/hole. On the side of a straight hole $n_r = 1$, $n_z = 0$, and on the flat surface closing the end of the hole/fiber $n_r = 0$, $n_z = 1$.

In the next step, a circular shape function is employed to approximate the variation in the temperatures and fluxes about the circumference of the fiber/hole using three nodes generated internally by the program around the user input nodes along the centerline of the fibers. The circular shape function is multiplied and integrated with the 3D kernel, so that the nodal values of variables can be brought outside the integral. Using the shape functions mentioned above, the temperature and flux can be expressed as

$$T = M^\gamma T^\gamma \quad q = M^\gamma q^\gamma \tag{10}$$

In the above expressions T^γ are nodal values of temperatures and q^γ are nodal values of fluxes respectively. The summation over γ is implied, $\gamma = 1, 2, 3$ for the three circumferential nodes.

The circular shape functions used in the current work are depicted in Fig. 2. They can be expressed as

$$\begin{aligned} M^1(\theta) &= \frac{1}{3} + \frac{2}{3}\cos\theta \\ M^2(\theta) &= \frac{1}{3} + \frac{\sqrt{3}}{3}\sin\theta - \frac{1}{3}\cos\theta \\ M^3(\theta) &= \frac{1}{3} - \frac{\sqrt{3}}{3}\sin\theta - \frac{1}{3}\cos\theta \end{aligned} \tag{11}$$

Also a modified shape function is used in the integration over the ends of the hole to ensure continuity temperature and flux at the center of the end surface which is given by

$$\overline{M}^\gamma = aM^\gamma + b/3, \quad \gamma = 1, 2, 3 \tag{12}$$

with

$$a = r/R \quad \text{and} \quad b = (R - r)/R \tag{13}$$

where R is the radius of the hole at the end; r is the location of the integration (Gauss) point as it sweeps from $r = 0$ to $r = R$; and M^γ is the circular shape function defined earlier.

The last term on the right-hand side of Eq. (5) can now be analytically integrated in the circumferential direction.

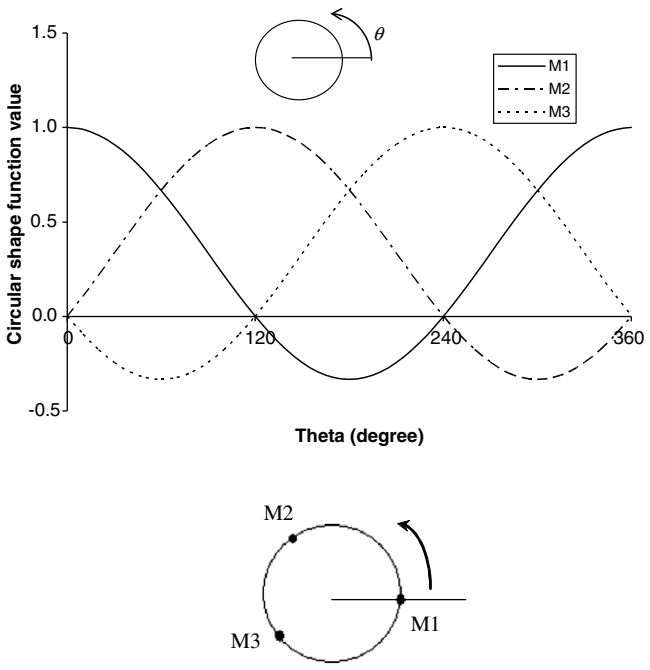

Fig. 2. Values of three nodal circular shape functions about the fiber/hole.

As an example, for the nth hole, the integrals can be expressed as

$$\begin{aligned} \int_{S^n} \overline{G}(x,\xi)q^{\mathrm{H}}(x)\,\mathrm{d}S^n(x) &= \int_{C^n}\int_0^{2\pi} \overline{G}^{\mathrm{local}}(R,\theta,z,\bar{\xi})M^\gamma R\,\mathrm{d}\theta q^\gamma\,\mathrm{d}C^n \\ &= \int_{C^n} \overline{G}^\gamma(R,z,\bar{\xi})q^\gamma\,\mathrm{d}C^n(z) \end{aligned} \tag{14}$$

where the integration over C^n as indicated above is now a simple one-dimensional curvilinear integration along the hole and G^γ represents the analytically integrated fiber/hole kernels.

The kernel functions of the fiber/hole resulting from the above analytical integration contain functions of elliptic integrals as defined in the Appendix. In general, these elliptic integrals are expressed numerically by common series approximations [6,8–11]. For a range of input values (coordinate locations), several higher order elliptical integral functions were found to produce inaccurate numerical results. To overcome this problem, several new series were derived using a best fit polynomial approximation (as a function of the modulus of elliptic integrals) using values of the integrals calculated by a very accurate numerical integration in the circumferential direction.

It should be pointed out that a fiber having curvature along its length will differ in surface area about the circumference on the curved portion of the fiber. This is neglected in the present formulation since the analytical integration is performed on an axisymmetric ring in which the surface area is constant about the circumference. This error, however, is small and disappears completely on a straight tubular fiber. For this reason, we cannot model an abrupt 90° bend on a fiber geometry.

4. Discretization

Once the integration in the circumferential direction is complete, a fiber in 3D solid can now be modeled as a 2D curvilinear line element with a prescribed radius at each longitudinal node with linear or quadratic variations of the field variables along the fiber elements. This requires finite discretization of the fibers in the longitudinal direction. Following usual discretization procedure [1], Eq. (4) can be discretized as

$$C^{\mathrm{F}}T(\xi) = -\sum_{p=1}^{P}\left[\int_{C^p} G^{F\gamma}(x,\xi)N^{\alpha}(\eta)\,\mathrm{d}C^p\right]q^{\alpha\gamma} + \sum_{p=1}^{P}\left[\int_{C^p} F^{H\gamma}(x,\xi)N^{\alpha}(\eta)\,\mathrm{d}C^p\right]T^{\alpha\gamma} \tag{15}$$

where, as mentioned above, the circumferential integration has already been performed analytically and P is the number of fiber elements. $N^{\alpha}(\eta)$ indicates a shape function over the curvilinear fiber element. Summation over α is implied. $q^{\alpha\gamma}$ and $T^{\alpha\gamma}$ are nodal values of flux and temperature on the surface of the fiber element, respectively.

In a similar fashion, Eq. (5) can be discretized using 1D (for the hole) and 2D (for the outer boundary) shape functions, which can be expressed as

$$CT(\xi) = \sum_{q=1}^{Q}\left[\int_{S^q} G^{\mathrm{O}}(x,\xi)L^{\beta}(\eta_1,\eta_2)\,\mathrm{d}S^q\right]q^{\beta} - \sum_{q=1}^{Q}\left[\int_{S^q} F^{\mathrm{O}}(x,\xi)L^{\beta}(\eta_1,\eta_2)\,\mathrm{d}S^q\right]T^{\beta} + \sum_{p=1}^{P}\left[\int_{C^p} \overline{G}^{\gamma}(x,\xi)N^{\alpha}(\eta)\,\mathrm{d}C^p\right]q^{\alpha\gamma} \tag{16}$$

where Q is the number of boundary elements on the outer surface of the matrix in the region; $L^{\beta}(\eta_1,\eta_2)$ represents a 2D shape function. Summation over β is implied; P is the number of fiber elements; q^{β} and T^{β} are nodal values of flux and temperature on the outer surface of the matrix, respectively; $q^{\alpha\gamma}$ and $T^{\alpha\gamma}$ are nodal values of flux and temperature on the surface of the hole, respectively.

It should be noticed that the temperatures and fluxes on a fiber/hole vary in the longitudinal as well as in the circumferential direction. For example, the temperature variations can be expressed as

$$T = M^{\gamma}N^{\alpha}T^{\alpha\gamma}$$

The circular shape function M^{γ} has been analytically integrated into the kernel functions of Eqs. (15) and (16). The ends of the fibers are assumed to be flat surface and a 1D numerical integration with respect to r is carried out in the radial direction. The coefficients obtained from the integration over the end are lumped with their respective coefficients from the integration of the side of the fiber.

5. Numerical integration

The complexity of the integral in the discretized Eqs. (15) and (16) necessitates the use of numerical integration for their evaluation. The steps involved in the numerical integration process for a given element are described briefly in the following paragraphs.

Using appropriate Jacobian transformations, a curvilinear fiber element or boundary element is mapped on a unit line or on a flat unit cell, respectively.

Depending on the proximity between the field point ξ and the element under consideration, element subdivisions and additional mapping are invoked.

Gaussian quadrature formulas are employed for the evaluation of the discretized integral over each element (or sub-element). These formulas approximate the integral as a sum of weighted function values at designated points. The error in the approximation is dependent on the order of the Gauss points employed in the formula. To minimize this error while at the same time maintaining computational efficiency, optimization schemes are used to choose the best number of gauss points for a particular field point and element [12–14].

When the field point coincides with a node of the element being integrated, the integration becomes singular. In that case, the value of the coefficients of the F kernel corresponding to the singular node cannot be evaluated accurately by the numerical integration. Instead, after the integration of all elements is complete, an equipotential technique [13] is applied to indirectly calculate the values of the singular terms. A discussion on these problems for 3D elastic bodies with holes and inclusions can be found in Banerjee and Henry [5] and Henry and Banerjee [6]. This equipotential technique when applied to the original intact boundary integral equation is often called regularization of the singularity.

6. Assembly of system equations

The approach to writing an efficient algorithm is to keep the number of system equations to a minimum by eliminating all unnecessary unknowns from the system. The strategy used in this work is to retain in the system only flux variables on the fiber–matrix interface. This is much more efficient than a general multi-region approach where both temperatures and fluxes are retained as unknowns on the interface. The elimination of the temperatures on the interface is achieved through a back-substitution of the fiber equations into the system equations which are formed exclusively from equations written for the matrix (on the outer surface and on the surface of the holes). The procedure is described below.

Eq. (16) is used to generate a system of equations for nodes on the outer surface of the composite matrix and for nodes on the surface of the holes containing fibers.

Written in matrix form, we have On the matrix outer surface:

$$G^{O}q^{O} - F^{O}T^{O} + \overline{G}q^{H} = 0 \tag{17a}$$

On the matrix hole surface:

$$G^{O}q^{O} - F^{O}T^{O} + \overline{G}q^{H} = IT^{H} \tag{17b}$$

where q^{O} and T^{O} are fluxes and temperatures on the outer surface of the matrix; q^{H} and T^{H} are fluxes and temperatures on the hole surface; I is the identity matrix; G^{O} and F^{O} matrices contain coefficients from the integration over the outer boundary $\overline{G}$ matrix contains coefficients integrated about the fiber/hole.

Our objective is to eliminate T^{H} from the system. To this end, Eq. (15) is written for every node on a fiber

$$G^{F2}q^{F} = F^{F2}T^{F}$$

In the above, superscript F2 identifies the equations written at points located at $r = 1.25$ times the fiber radius (where $C^{F}_{ij} = 0$) as the boundary is approached from outside the fiber region.

Noting $T^{H} = T^{F}$, and $q^{H} = -q^{F}$ we have

$$F^{F2}T^{H} = -G^{F2}q^{H} \tag{18}$$

Pre-multiplication of Eq. (17b) by the F^{F2} matrix yields

$$F^{F2}G^{O}q^{O} - F^{F2}F^{O}T^{O} + F^{F2}\overline{G}q^{H} = F^{F2}T^{H} \tag{19}$$

Eq. (18) can now be set equal to Eq. (19) and the final form of the system is derived.

On the outer surface:

$$G^{O}q^{O} - F^{O}T^{O} + \overline{G}q^{H} = 0 \tag{20a}$$

On the hole surface:

$$F^{F2}G^{O}q^{O} - F^{F2}F^{O}T^{O} + (F^{F2}\overline{G} + G^{F2})q^{H} = 0 \tag{20b}$$

At every point on the outer surface, either the flux or the temperature is specified and on the outer surface of the hole only fluxes are retained. Therefore, the number of equations in the system is equal to the final number of unknowns, and hence, the system can be solved. Thereafter, (17b) is used to determine the temperature on the fiber–matrix interface.

It should be noted that since the temperature about a particular hole is present only in the fiber equation corresponding to that hole, back-substitution can be performed for one fiber at a time in a more efficient manner than back-substitution of all fibers at once. Further, nowhere in the assembly process is a matrix inversion necessary. This efficient assembly process was made possible due to the unique formulation of the modified boundary integral equations derived in Section 2.

When the composite matrix is divided into a multi-region model, the above fiber assembly can be performed for each region independently. Thereafter, equilibrium and compatibility conditions are invoked at common interfaces of the sub-structured matrix composite. After collecting together the known and unknown boundary quantities, the final system can be expressed as

$$A^{b}x = B^{b}y \tag{21}$$

where x is the vector of unknown variables on the outer boundary and unknown fluxes along the fiber–matrix interface; y is the vector of known variables on the outer boundary of the composite matrix; A^{b} and B^{b} are associated coefficient matrices

7. Interior quantities

Once all of the temperatures and fluxes are known on the matrix outer surface and on the fiber–matrix interface, interior quantities can be determined at any point in the composite matrix or fiber. For temperature, either the conventional boundary temperature integral Eq. (1) or (2) can be employed or alternatively, the modified Eq. (4) or (5) can be used.

For example, the interior flux within the composite matrix can be determined using the modified boundary integral Eq. (5) as

$$\begin{aligned} q_i(\xi) = &\sum_{q=1}^{Q}\left[\int_{S^q} E_i^{O}(x,\xi)L^{\beta}(\eta_1,\eta_2)\,dS^q(x)\right]q^{\beta} \\ &- \sum_{q=1}^{Q}\left[\int_{S^q} D_i^{O}(x,\xi)L^{\beta}(\eta_1,\eta_2)\,dS^q(x)\right]T^{\beta} \\ &+ \sum_{p=1}^{P}\left[\int_{C^p} \overline{E}_i^{H\gamma}(x,\xi)N^{\alpha}(\eta)\,dC^p(x)\right]T^{\alpha\gamma} \end{aligned} \tag{22}$$

where

$$E_i = -k\frac{\partial G}{\partial \xi_i} \tag{23}$$

$$D_i = -k\frac{\partial F}{\partial \xi_i} \tag{24}$$

$$\overline{E}_i = -k\frac{\partial \overline{G}}{\partial \xi_i} \tag{25}$$

In Eqs. (23)–(25), k denotes the conductivity, q is the flux, T is the temperature and G and F are temperature and flux kernels, respectively, defined before.

A similar equation can be written for the heat flux inside a fiber. These equations, however, are only valid for interior points, whereas, when ξ is on the boundary, known values of temperature, fluxes and shape functions can be used together with the following relationships, to determine the heat flux.

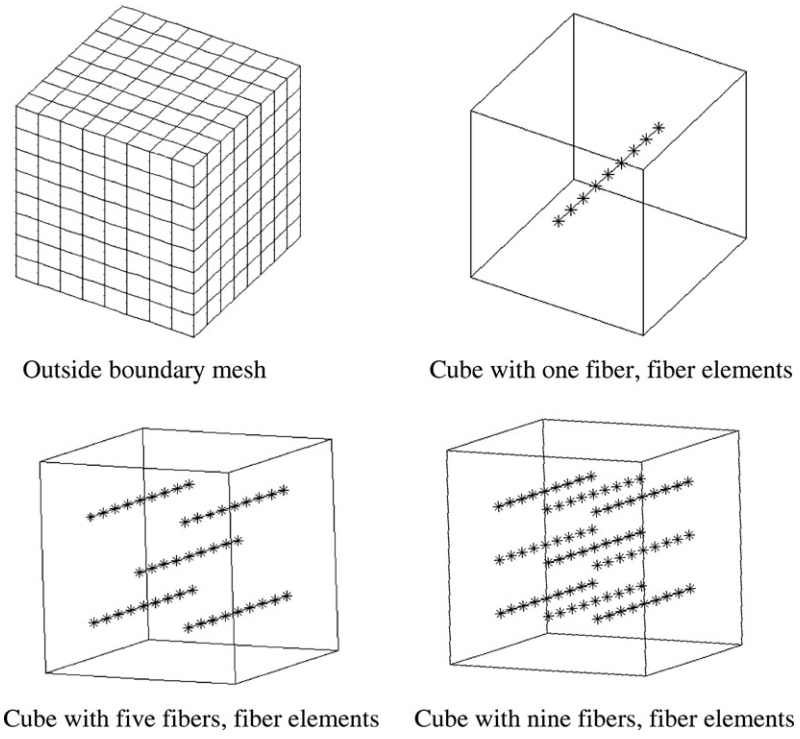

Fig. 3. Unit cube with one, five and nine fibers BEM meshes for fiber element formulation.

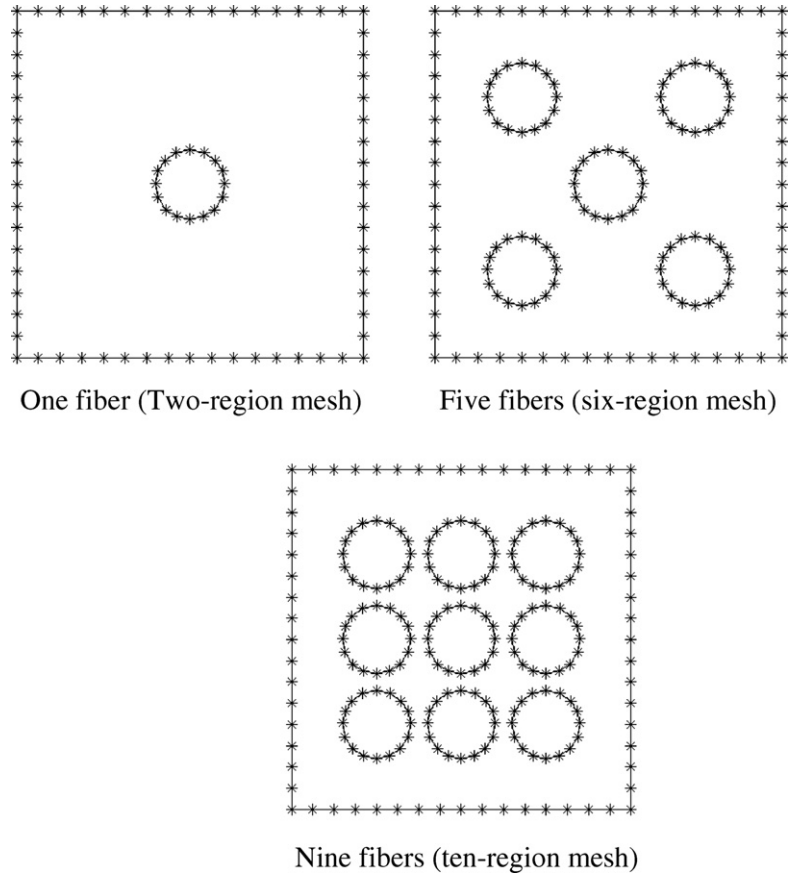

Fig. 4. Unit cube with one, five and nine fibers 2D plane strain multi-region BEM meshes.

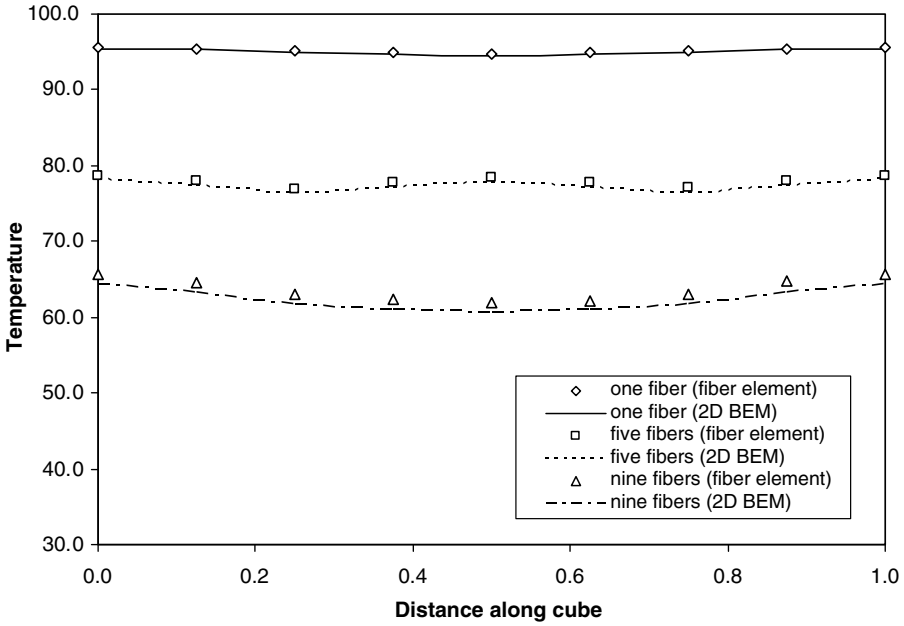

Fig. 5. Unit cube with one, five and nine fibers, temperature profile.

Table 1
Precision comparison with different radii (cube with nine fibers)

Distance along cube	Case A: radius = 0.1			Case B: radius = 0.05		
	2D BEM	Fiber element	Error (%)	2D BEM	Fiber element	Error (%)
0	64.3	65.7	2.1	89.8	90.0	0.2
0.125	63.3	64.7	2.2	89.5	89.7	0.2
0.25	61.7	62.9	1.9	88.9	89.2	0.3
0.375	61.0	62.2	1.9	88.7	88.9	0.2
0.5	60.7	61.9	1.9	88.5	88.8	0.3
0.625	61.0	62.3	2.1	88.7	88.9	0.2
0.75	61.7	63.0	2.1	88.9	89.2	0.3
0.875	63.3	64.6	2.0	89.5	89.7	0.2
1	64.3	65.6	2.0	89.8	90.0	0.2

Table 2
CPU time comparison for different meshes

Analysis	Modeling mesh	CPU time (s)
Fiber modeling	24 Boundary elements, one 4-element insert	1.5
	96 Boundary elements, one 4-element insert	5.8
	96 Boundary elements, five 4-element inserts	9.8
3D multi-region BEM modeling	96 Boundary elements, 32 elements on insert surface (one cylinder)	9.5

$$q_i = -k\frac{\partial T}{\partial x_i} \tag{26}$$

$$\frac{\partial T}{\partial x_j}\frac{\partial x_j}{\partial \eta_i} = \frac{\partial T}{\partial \eta_i} \tag{27}$$

8. Numerical accuracy and efficiency

8.1. Introduction

In order to test the validity of the proposed formulation, several numerical examples are presented using fiber element formulation for steady-state heat conduction analysis. The numerical results obtained using the present algorithm are compared with those of multi-region BEM and other available solutions. As mentioned earlier, the use of multi-region BEM for fibers of small diameter becomes progressively inaccurate as the fiber diameter decreases while the present fiber element approximation becomes more accurate for the smaller diameter fiber. In the following verification examples, we have chosen the

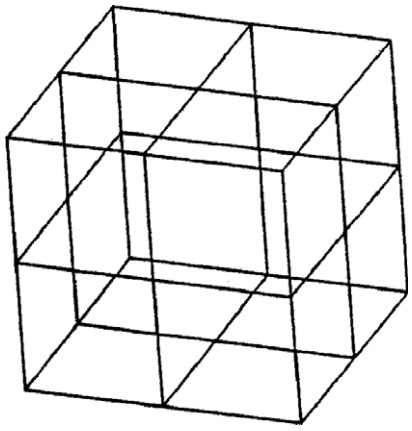

Fig. 6. Effective conductivity of a cube with nine fibers, BEM mesh used for the outer boundary (fiber elements not shown).

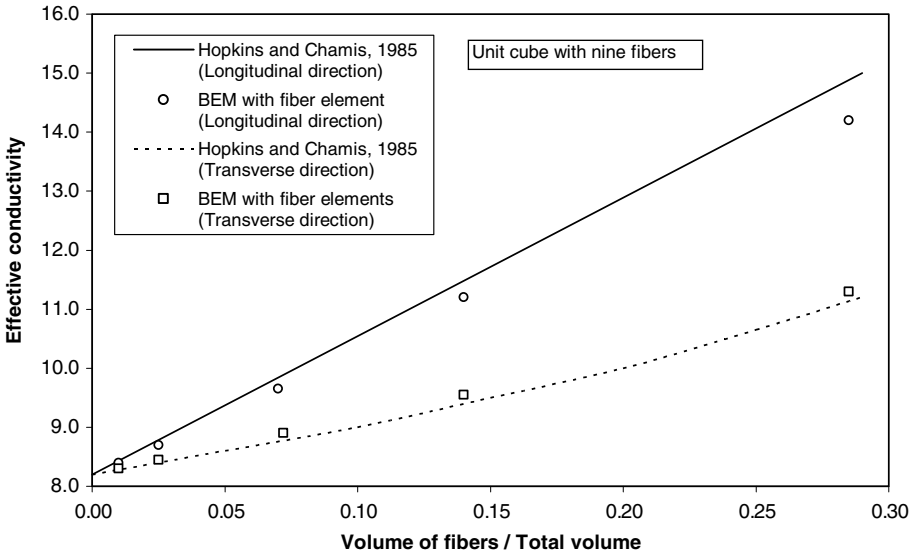

Fig. 7. Effective conductivity in a cube for various fiber diameters.

diameters of the fibers such that the multi-region BEM remains the most accurate results.

8.2. Cube with one, five and nine fibers

In this first verification example, the steady-state heat flow through a 3D unit cube with one, five and nine fibers is studied. The conductivity of the fibers is assumed to be 10 times the conductivity of the matrix material. The radius of each fiber is taken as 0.1 for Case A and 0.05 for Case B. A uniform flux of 100.0 is applied to a side of the cube parallel to the fibers. The opposite side of the cube is maintained at a temperature of 0 °C. All other faces of the cube are insulated.

The BEM meshes used in this problem for the 3D fiber element formulation are shown in Fig. 3 and the corresponding multi-region 2D BEM meshes are shown in Fig. 4. The outside boundary mesh for the fiber element formulation consists of 384 eight-noded quadratic elements (64 elements on each face), whereas, 4 three-noded quadratic elements are used to model each fiber as shown in Fig. 3. The 2D BEM meshes uses 3-noded quadratic elements on the boundary and on the surface of the holes and fibers as depicted in Fig. 4.

The resulting temperature profiles on the face subjected to flux are shown in Fig. 5 for three fiber arrangements. The numerical results of the fiber element formulation are seen to be in excellent agreement with the corresponding 2D multi-region BEM results. Here, the effect of the number of fibers on the temperature profile is of particular interest. As the number of fibers is increased, the overall conductivity of the cube is increased. Hence, the heat from the applied flux is carried away (to the face which is maintained at 0 °C) at a higher rate, resulting in lower temperatures. Also note, the local temperature minimums in the temperature profiles are associated with the close proximity of the fibers near the flux boundary.

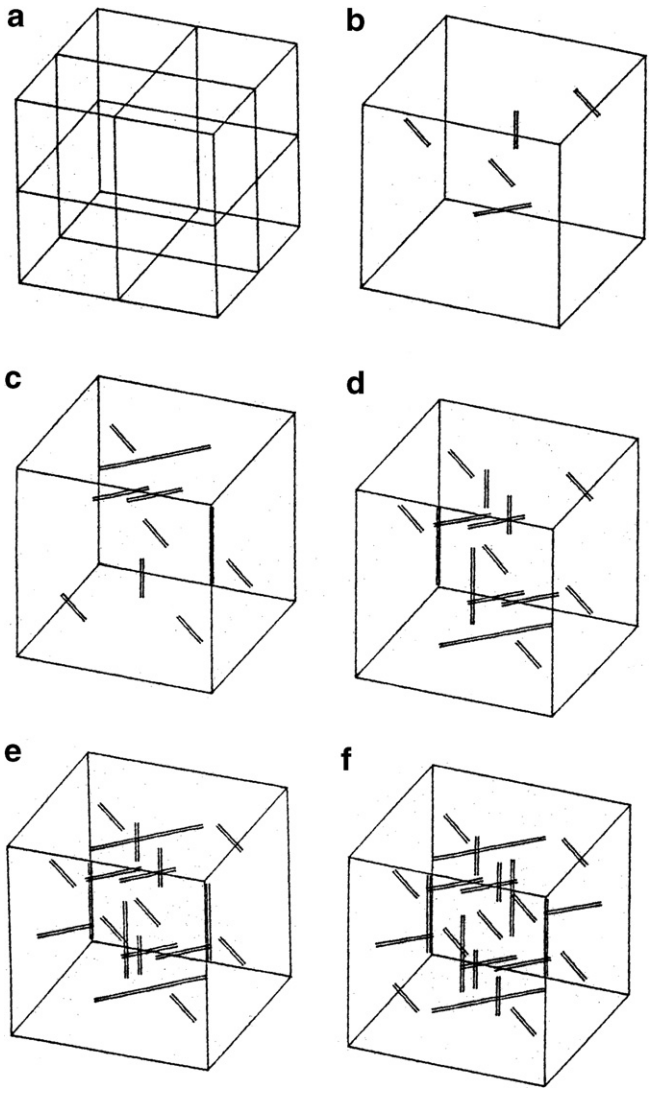

Fig. 8. Cube with random fibers: (a) surface discretization; (b–f) orientation of variable length fibers within the unit cube containing 5, 10, 15, 20 and 25 fibers, respectively.

In order to illustrate the effects of the fiber radius on the accuracy of the results of 3D fiber modeling and the 2D multi-region modeling, the temperature distribution along the face subjected to flux are listed in Table 1 for different fiber radii. It shows that the present fiber modeling becomes more accurate for the smaller radius (0.05), even the results for the larger radius (0.1) are quite acceptable.

For the demonstration of the computation efficiency, a full 3D multi-region modeling was done for the problem of one fiber inclusion (since the modeling effort for more fibers as multi-region problem would have consumed a very large amount of modeling effort). The CPU times on HP B2000 Workstation are summarized in Table 2. All of the models here lead to the same numerical results. It is important to note that in addition to the vastly reduced modeling effort, the CPU times of the line element fiber modeling are significantly small. This advantage of course is likely to be magnified in problems in which a large number of fibers exist.

8.3. Heat conduction: effective conductivity in a fiber composite

In the present example, the conductivity of heat flow in a unit cube with nine fibers is investigated. The outside boundary mesh of the 3D BEM model utilized in this example is shown in Fig. 6. In this problem, 24 elements are used to model the outer boundary whereas, each of the nine fibers is modeled using 1 three-noded fiber element. The fibers are assumed to be perfectly bonded to the matrix so that the resistance of the heat flow across the interface is zero. The cube is subjected to a temperature of 0 °F on a face perpendicular to the fibers and 100 °F on the opposite face. The remaining four faces are insulated. The total heat flux through the cube is calculated and the effective conductivity in the direction parallel to the fibers is then found. When the boundary conditions are rearranged to produce heat flow perpendicular to the fibers, the effective conductivity in the transverse direction can also be determined. The specified radius of the fibers is changed to simulate different void ratios, therefore minimizing the effort required for re-analysis of the cube with different fiber to total volume ratios. This illustrates the main convenience of the present formulation for the micro-mechanical analysis.

The fiber composite has the following conductivities

$$k_{\text{matrix}} = 8.2 \quad \text{Btu/h ft F}(14.19\ \text{W/m C})$$
$$k_{\text{fiber}} = 32.0 \quad \text{Btu/h ft F}(55.38\ \text{W/m C})$$

In Fig. 7, the effective conductivities in both the lateral and transverse directions are shown as a function of the ratio of the fiber volume to the total volume of the composite specimen. The solutions generally are in good agreement with the approximate solutions by Hopkins and Chamis [15] at low fiber to total volume ratios and slightly deviate from one another when the fiber to total volume ratio is large. It should be noted that Hopkins and Chamis [15] have essentially used the theory of mixture in their derivation in which the effect of multiple fiber interacting with each other through the matrix is not present in their theory. Hence the present results which include this interaction are likely to be more relevant.

8.4. Heat flow in a cube with random fibers

Next, we analyze the heat flow in a unit cube with randomly oriented fibers as shown in Fig. 8. In this analysis, the left end of the cube is subjected to a prescribed temper-

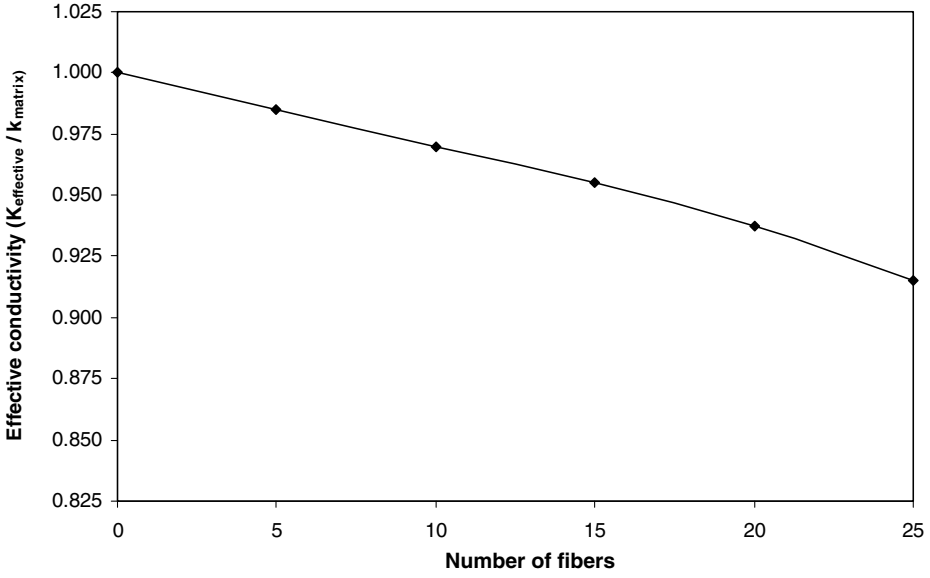

Fig. 9. Effective conductivity in a cube with random fibers.

ature of 100 °C and for the right end, a temperature of 0 °C is specified. All other surfaces are assumed to be insulated.

Fig. 9 shows the equivalent thermal conductivity of the cube for different fiber arrangements. In this analysis, the thermal conductivity of the matrix is assumed to be 100 times more than the conductivity of the fibers.

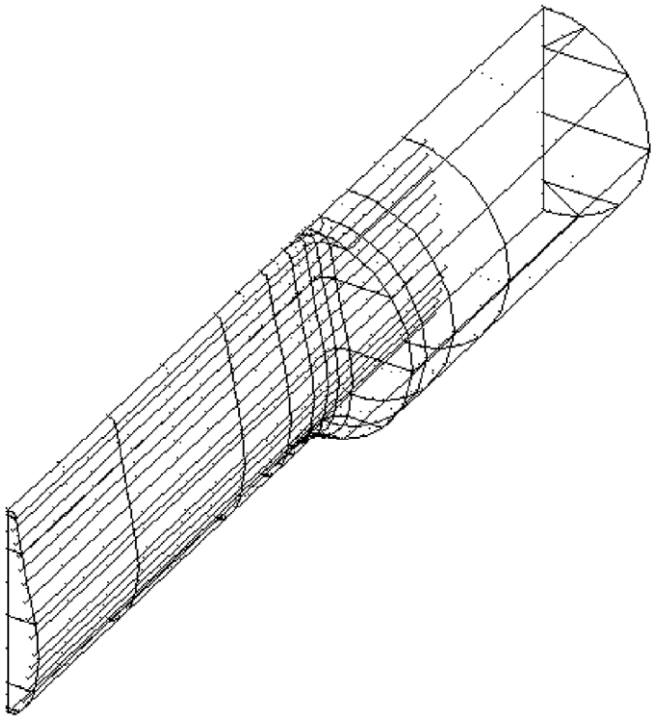

Fig. 10. Fiber reinforced turbine blade, BEM mesh.

9. An example of application

In this example, an attempt has been made to apply the present fiber element formulation to steady-state heat conduction analysis of a turbine blade. A boundary element discretization of a turbine blade with fibers is shown in Fig. 10. Half symmetry is employed in this model which consists of 92 quadratic elements on the outer boundary. The model is 58.2 mm long, 13.9 mm wide, the radius of the base is 6.95 mm, and the tip is 1.98 mm (from the plane of symmetry) in thickness at the largest point. The blade also consists of 26 fibers (13 fibers per side) running from the tip of the blade to half way through the base as shown in Figs. 8 and 9. The radius of each fiber is 0.15 mm. Seven quadratic fiber elements are used to model each fiber and thus the total number of fiber elements used in this problem is 92. The conductivity of the blade is 0.0216 W/mm °C and the conductivity of the fibers is 100 times the conductivity of the blade. A gas at a temperature of 1200 °C is assumed to flow over the blade while a gas at a temperature of 500 °C surrounds the base of the blade. The difference between the surface temperature and the ambient is assumed to be linearly related to the heat flux via a film coefficient which can be expressed as

$$Q = -h(T_a - T)$$

where, Q is the heat flux, T and T_a are surface temperature and ambient temperature, respectively. Q is positive if heat

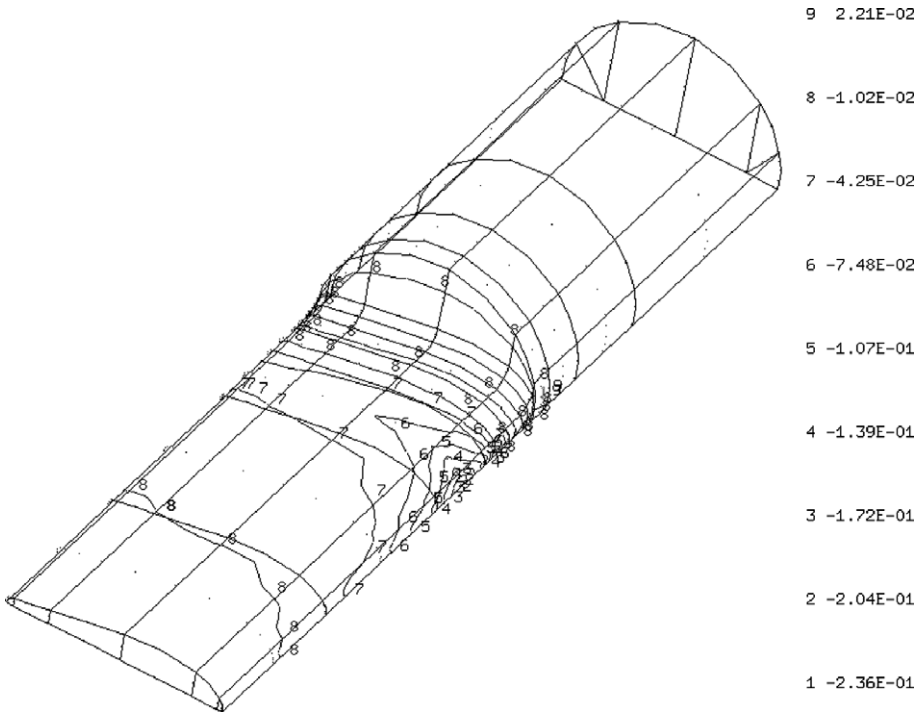

Fig. 11. Distribution of heat flux at steady-state for the homogeneous blade.

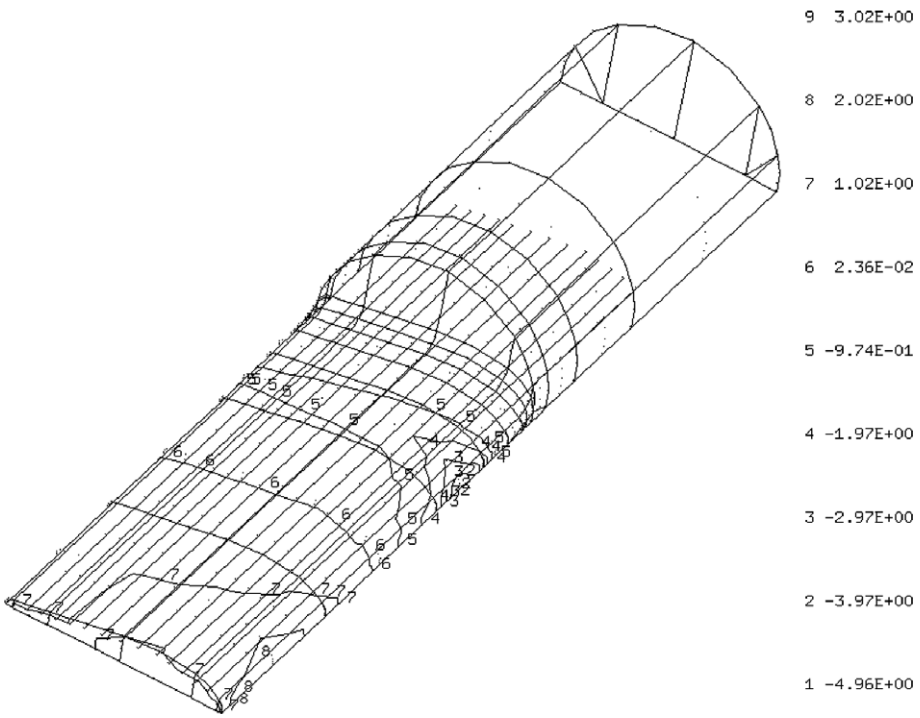

Fig. 12. Distribution of heat flux at steady-state for fiber reinforced blade.

is leaving the body and is negative when heat is entering the body. Using this type of boundary condition, Q is not specified, but its value is determined from h, T_a and the unknown temperature at the surface T.

In this problem, at the leading edge of the blade a film coefficient is $h = 0.003395$ W/mm^2 °C and tapers off to $h = 0.00064$ W/mm^2 °C at the trailing edge. At the base of the blade the film coefficient of $h = 0.00005$ W/mm^2 °C is assumed.

A steady-state heat conduction analysis is first carried out on a homogeneous blade (no fiber) with a conductivity of 0.0216 W/mm °C. The resulting heat flux distribution is shown in Fig. 11.

Then the blade is re-analyzed with fibers and the corresponding steady-state heat flux distribution is presented in Fig. 12. As expected, the overall higher conductivity of the fibers increases the heat flow through the blade from the tip towards the base, resulting in a different heat flux distribution as compared to the homogeneous blade.

10. Conclusions

An efficient and comprehensive BEM formulation for the steady-state 3D heat conduction analysis of composites has been developed. The analysis is shown to be sufficiently accurate and can be applied to solve realistic practical problems of different scale.

An attractive feature of the present implementation lies in the fact that the arrangements of fibers can be altered with relative ease thus avoiding the effort for remodeling. Also, various fiber to matrix ratios can be simulated just by changing the fiber radius. All of these features result in significant savings in computing cost and time.

Acknowledgement

We are deeply indebted to BEST Corporation of Getzville, New York for making available several blocks of General Purpose Boundary Element Software Technology (GPBEST) system for this development.

Appendix A

This Appendix discusses about the analytically integrated kernel functions of the fiber/hole about the circumference.

Referring to Fig. 13, let (r_x, θ_x, z_x) and $(r_\xi, \theta_\xi, z_\xi)$ are the coordinates of the field point x and the source point ξ, respectively. The locations of the three nodes on the circumference for the circular shape function are presented in Fig. 2. After expressing the kernel functions in local coordinates with the center of the coordinate system coinciding with the center of the hole/fiber and the z-axis aligned with the centerline of the fiber, as described in Section 3, using the above notations the analytically integrated temperature and flux kernels are presented below.

A.1. Analytically integrated temperature kernel

The product of the free space Green's function and the circular shape function (defined in Section 3) can be analytically integrated with respect to θ_x resulting the following

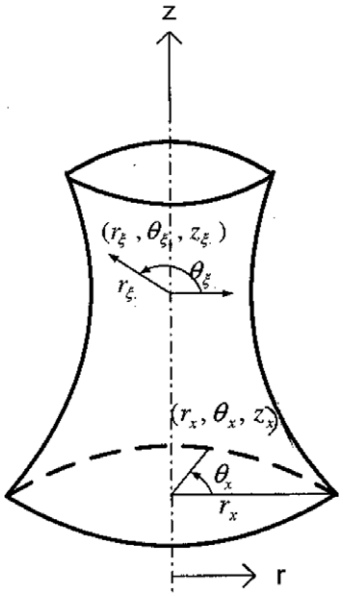

Fig. 13. A body in cylindrical coordinate system.

expressions for the three values of G^γ with $\gamma = 1, 2, 3$ (corresponding to the three values of $\theta_\xi = 0, +\frac{2\pi}{3}$ and $-\frac{2\pi}{3}$)

$$G^1 = \frac{1}{3}\frac{R}{4\pi k}P_1 + \left(\frac{2}{3}\cos\theta_\xi\right)\frac{R}{4\pi k}P_2$$

$$G^2 = \frac{1}{3}\frac{R}{4\pi k}P_1 + \left(\frac{\sqrt{3}}{3}\sin\theta_\xi - \frac{1}{3}\cos\theta_\xi\right)\frac{R}{4\pi k}P_2$$

$$G^3 = \frac{1}{3}\frac{R}{4\pi k}P_1 + \left(-\frac{\sqrt{3}}{3}\sin\theta_\xi - \frac{1}{3}\cos\theta_\xi\right)\frac{R}{4\pi k}P_2$$

In the above expressions, k is the conductivity and R is the radius of the fiber/hole. The terms P_1 and P_2 are functions of elliptic integrals defined as

$$P_1 = \int_0^{2\pi}\frac{\mathrm{d}\theta}{r} = 4C_1/R_d$$

$$P_2 = \int_0^{2\pi}\frac{\cos\theta\,\mathrm{d}\theta}{r} = -4(2C_2 - C_1)/R_d$$

with

$$C_1 = \int_0^{\pi/2}\frac{\mathrm{d}\theta}{(1 - m\sin^2\theta)^{1/2}} = \kappa$$

$$C_2 = \int_0^{\pi/2}\frac{\cos^2\theta\,\mathrm{d}\theta}{(1 - m\sin^2\theta)^{1/2}} = (\varepsilon - m_1\kappa)/m$$

$$r(x,\xi) = R_d\left[1 - \frac{m}{2}(1 + \cos\theta)\right]^{1/2} = R_d\left(1 - m\sin^2\frac{\theta}{2}\right)^{1/2}$$

$$R_d = [(r_x + r_\xi)^2 + (z_x - z_\xi)^2]^{1/2}$$

where the modulus m and the complementary modulus m_1 of the elliptical integrals are given by

$$m = \frac{4r_x r_\xi}{R_d^2}$$

$$m_1 = 1 - m$$

In the above expressions, κ and ε are elliptic integrals of first and second kind [9] given by

$$\kappa = \int_0^{\pi/2}\frac{\mathrm{d}\theta}{(1 - m\sin^2\theta)^{1/2}}$$

$$\varepsilon = \int_0^{\pi/2}(1 - m\sin^2\theta)^{1/2}\,\mathrm{d}\theta$$

which can be approximated by polynomial approximations defined in Abramowitz and Stegun [8].

A.2. Analytically integrated flux kernel

For the flux kernel, the analytically integrated expressions (F^γ) can be expressed as

$$F^1 = \frac{1}{3}[Q_1F_2 + Q_2F_1] + \left(\frac{2}{3}\cos\theta_\xi\right) \times [Q_1F_3 + Q_2F_2]$$

$$F^1 = \frac{1}{3}[Q_1F_2 + Q_2F_1] + \left(\frac{\sqrt{3}}{3}\sin\theta_\xi - \frac{1}{3}\cos\theta_\xi\right) \times [Q_1F_3 + Q_2F_2]$$

$$F^1 = \frac{1}{3}[Q_1F_2 + Q_2F_1] + \left(-\frac{\sqrt{3}}{3}\sin\theta_\xi - \frac{1}{3}\cos\theta_\xi\right) \times [Q_1F_3 + Q_2F_2]$$

In the above expressions

$$Q_1 = -\frac{R}{4\pi k}R_\mathrm{L}n_r \quad \text{and} \quad Q_2 = \frac{R}{4\pi k}[Rn_r + (z_x - z_\xi)n_z]$$

where, the term R_L represents the relative translation added to the field coordinate (see Section 3, Eq. (7)), n_r and n_z are normals in local coordinates at the integration points and the other terms have their usual meanings defined earlier.

The terms F_1, F_2 and F_3 are functions of elliptic integrals defined as

$$F_1 = \int_0^{2\pi}\frac{\mathrm{d}\theta}{r^3} = 4A_1/R_\mathrm{d}^3$$

$$F_2 = \int_0^{2\pi}\frac{\cos\theta\,\mathrm{d}\theta}{r^3} = -4(2A_2 - A_1)/R_\mathrm{d}^3$$

$$F_3 = \int_0^{2\pi}\frac{[(\cos\theta - \sin\theta)^2 - 2\sin^2\theta\cos^2\theta]\,\mathrm{d}\theta}{r^3} = 4(4A_3 - 4A_2 + A_1)/R_\mathrm{d}^3$$

with

$$A_1 = \int_0^{\pi/2} \frac{\mathrm{d}\theta}{(1 - m\sin^2\theta)^{3/2}} = \frac{\varepsilon}{m_1}$$

$$A_2 = \int_0^{\pi/2} \frac{\cos^2\theta\,\mathrm{d}\theta}{(1 - m\sin^2\theta)^{3/2}} = \frac{\kappa - \varepsilon}{m}$$

$$A_3 = \int_0^{\pi/2} \frac{\cos^4\theta\,\mathrm{d}\theta}{(1 - m\sin^2\theta)^{3/2}} = [\varepsilon(1 + m_1) - 2m_1\kappa]/m^2$$

where, the terms have their usual meanings defined earlier.

These expressions can be then integrated with respect to r to provide the contributions of the end disc (refer to Section 3, Eq. (13)) and also with respect to z for the longitudinal direction.

References

[1] P.K. Banerjee, The Boundary Element Methods in Engineering, McGraw-Hill, London, 1994.

[2] G.F. Dargush, Boundary Element Methods for the Analogous Problems of Thermomechanics and Soil Consolidation, Ph.D. Dissertation, State University of New York at Buffalo, Buffalo, New York, 1987.

[3] G.F. Dargush, P.K. Banerjee, Advanced development of the boundary element method for steady-state heat conduction, Int. J. Numer. Meth. Eng. 28 (1989) 2123–2142.

[4] G.F. Dargush, P.K. Banerjee, Application of boundary element to transient heat conduction, Int. J. Numer. Meth. Eng. 31 (1991) 1231–1248.

[5] P.K. Banerjee, D.P. Henry, Elastic analysis of three-dimensional solids with fiber inclusions by BEM, Int. J. Solids. Struct. 29 (1992) 2423–2440.

[6] D.P. Henry, P.K. Banerjee, Elastic analysis of three-dimensional solids with small holes by BEM, Int. J. Numer. Meth. Eng. 31 (1991) 369–384.

[7] M.R. Barone, D.A. Caulk, Special boundary integral equations for approximate solution of potential problems in three-dimensional regions with slender cavities of circular cross-section, IMA J. Appl. Math. 35 (1985) 311–325.

[8] M. Abramowitz, I.A. Stegun, Handbook of Mathematical Functions, Dover, New York, 1974.

[9] P.F. Byrd, M.D. Friedman, Handbook of Elliptical Integrals for Engineers and Physicists, Springer, Berlin, 1954.

[10] H.C. Wang, A General Purpose Development of BEM for Axisymmetric Solids, Ph.D. Dissertation, State University of New York at Buffalo, Buffalo, New York, 1989.

[11] H.C. Wang, P.K. Banerjee, Multi-domain general axisymmetric stress analysis by BEM, Int. J. Numer. Meth. Eng. 28 (1989) 2065–2083.

[12] J.O. Watson, Advanced implementation of the BEM for two and three-dimensional elastostatics, in: P.K. Banerjee, R. Butterfield (Eds.), Developments in Boundary Element Methods-1, Elsevier Applied Science, London, 1979, pp. 31–63.

[13] P.K. Banerjee, R. Butterfield, Boundary Element Methods in Engineering Science, McGraw-Hill, London, 1981.

[14] P.K. Banerjee, R.B. Wilson, N. Miller, Advanced elastic and inelastic stress analysis of gas turbine engine structures by BEM, Int. J. Numer. Meth. Eng. 26 (1988) 393–411.

[15] D.A. Hopkins, C.C. Chamis, A unique set of micromechanical equation for high temperature metal matrix composites, in: First Symposium on Testing Technology of Metal Matrix Composites, Nashville, TN, 1985.

[16] N. Nishimura, Y.L. Liu, Thermal analysis of carbon-nanotube composites using a rigid-line inclusion model by boundary integral equation method, Comput. Mech. 35 (2004) 1–10.